Proton mean-free path in nuclear matter and in finite nuclei

H. J. Yuan, H. L. Lin, and G. Fai

Department of Physics, Kent State University, Kent, Ohio 44242

S. A. Moszkowski

Department of Physics, University of California at Los Angeles, Los Angeles, California 90024
(Received 20 March 1989)

The mean-free path of protons is calculated in nuclear matter and in finite nuclei using the extended Skyrme interaction. The Green's function technique is employed for infinite nuclear matter to carry out the calculations analytically. The connection to finite nuclei is established and results are compared to data extracted from reaction cross sections and optical-potential fits for three closed-shell nuclei. Fixing the radius parameter as in the interpretation of the measurements leads to reasonable agreement within the accuracy of the data.

I. INTRODUCTION

The mean-free path of the constituents is a fundamental property of a many-body system. In the case of the propagation of a nucleon through the nucleus, the data indicate that the mean-free path is of the order of 4–6 fm for protons of energy $E_p = 50$–200 MeV.[1-5] The relatively long mean-free path of the nucleons implies a smooth average potential, upon which the well-known independent-particle model is based. The nucleon mean-free path is also a crucial parameter in theoretical treatments of nuclear collisions, which explore nuclear matter away from zero temperature and normal nuclear density.[6-8] In the present paper, we restrict our attention to densities up to that of normal nuclear matter and to zero temperature.

According to the standard kinetic argument, the nucleon mean-free path in nuclear matter can be written as $\lambda_0 = (\bar{\sigma}\rho)^{-1}$, where $\bar{\sigma}$ is the nucleon-nucleon cross section and ρ is the density of nuclear matter. The kinetic argument is based entirely on the density of the medium, and is typically used with the free experimental average nucleon-nucleon cross section. This simple estimate yields ≈ 1–2 fm for the mean-free path of protons in normal nuclear matter in the energy region considered here ($E_p = 50$–200 MeV).[4] To obtain a longer mean-free path theoretically, one needs to take into account the specific properties of the nuclear medium. It is well known that, e.g., the Pauli principle acts to enlarge the mean-free path, and this increase leads to representative values for λ in the range 2.5–3 fm.[9,10] Recently, the effect of the nonlocality of the nucleon propagating through the nuclear medium was incorporated in calculations of the mean-free path.[11-14] To set the stage for the present calculation, in Sec. II we will qualitatively review the effects that increase λ_0.

The aim of this paper is to explore a microscopic calculation of the nucleon mean-free path based on the extended Skyrme interaction.[15-19] Skyrme forces have been used successfully as effective interactions in nuclear struc-

ture calculations for many years (see, e.g., Ref. 20). Their simplicity has provided an enormous computational advantage over realistic nucleon-nucleon forces, while yielding a comparable fit to bound-state properties.[19] The extended Skyrme interaction was recently shown to give promising results also in the area of optical-model calculations.[21,22]

The extended Skyrme interaction, which has a finite-range density dependence, gives better fits to nuclear properties (in particular to nuclear spectra), than conventional Skyrme forces with a zero-range density dependence.[15-19] Indeed, to a good approximation, the density-dependent term has the same range as the density-independent term. This is suggestive of a model where the density-independent two-body interaction is multiplied by a function of the local density. Such a model leads to good fits to spectra of nuclei in the s-d shell.[23]

It is realized that Skyrme interactions were designed with a rather limited scope of applications in mind. We feel, however, that the previously mentioned successes invite applications in other areas. In particular, we would like to assess the potential of the extended Skyrme interaction in calculations of the mean-free path. As our calculational method, we employ the Green's function technique, the efficiency of which was recently demonstrated in applications to the optical potential and to single-particle spreading widths.[21,24] One of the advantages of this approach is that the Fermi motion of the nucleons and the Pauli principle are automatically built in from the beginning.

A full calculation of the optical potential (which in turn determines the mean-free path) should ideally be based on a g-matrix approach using one of the modern nucleon-nucleon potentials (e.g., the Paris,[25] or the Bonn[26] potential). Such numerical calculations are naturally quite elaborate.[27] For an estimate of the mean-free path, in particular in view of the uncertainty with respect to the free nucleon-nucleon force, it appears to be more economic to use an *effective* force. The Skyrme interac-

tion represents an expansion of both the range and the nonlocality of a realistic interaction through second order in momentum space, i.e., only terms of order p^0 and p^2 are kept. This is equivalent to making a short-range expansion in coordinate space and keeping only the lowest two moments.

Since the Skyrme interaction is an effective force, care must be taken in evaluating higher-order diagrams, such as the second-order diagrams for the imaginary part of the optical potential. We expect that here, just as in the case of the real part, the lowest-order nonvanishing diagrams will give the main contribution, mocking up higher-order effects. Considerable progress has already been made in relating the Skyrme interaction to the g matrix for a realistic interaction.[28] Further work along these lines is clearly important, but is outside the scope of the present paper.

The extended Skyrme interaction[19] can also be used to calculate the nuclear incompressibility and the mean field, which are key elements of the nuclear equation of state and of dynamical descriptions of nucleus-nucleus collisions. In the present work we focus on the mean-free path as a specific example of the quantities of interest.

In Sec. III the extended Skyrme interaction is introduced briefly, and the elements of the Green's function approach are reviewed. The section ends with a discussion of the imaginary part of the optical potential and the mean-free path. Section IV first presents our results for nuclear matter. The connection to finite nuclei is established via the local density approximation and comparisons to data are displayed. The parameters of the Skyrme interaction used here are identical to those successfully used in bound-state and optical-potential calculations.[19,21] Our findings are summarized in Sec. V. Calculational details are relegated to the Appendixes.

II. QUALITATIVE ESTIMATES

In the energy range of our interest (up to 200 MeV), the total (elastic) cross section for nucleon-nuleon scattering in free space (averaged over isospin) can be roughly represented by

$$\bar{\sigma} \approx \frac{600}{E} , \tag{1}$$

where E is the laboratory energy in MeV, and the cross section is given in units of fm^2.[4] Using $\rho = 0.16/\text{fm}^3$ for normal nuclear matter density, we then obtain from the standard kinetic argument for the mean-free path of a nucleon in nuclear matter

$$\lambda_0 = \frac{1}{\bar{\sigma}\rho} \approx 0.01E , \tag{2}$$

i.e., 1 fm for a nucleon of 100 MeV.

The effect of the nuclear medium is completely neglected (apart from the numerical value of its density) in this argument. Physically, it is easy to recognize three different (but not independent) ways in which the nuclear medium increases the nucleon mean-free path: (1) by the reduction of the nucleon mass (effective mass), (2) by the explicit density dependence of the nucleon-nucleon interaction used (density dependence), and (3) by the blocking of occupied states (Pauli principle). To gain insight, here we discuss each of these qualitatively and give a crude estimate of each effect. Since the effects are not independent, some double counting is expected at this level. More detailed calculations are described in the remaining sections of the paper. Similar discussions for higher densities, where other ingredients also come into play, have been given recently in the context of nuclear collisions. (See, e.g., Ref. 29).

A. Effective mass

A reduction of the effective mass of the nucleon, due to the nonlocality of the single-particle potential, spreads out the single-particle levels. This reduces the effective cross sections. In particular, the imaginary potential W contains a multiplicative factor m^*. Now, as will be discussed in Sec. III C, the mean-free path can be written as the mean lifetime (proportional to $1/W$) times the group velocity. Since the group velocity is inversely proportional to m^*, we have

$$\lambda \sim \lambda_0/m^{*2} \tag{3}$$

where λ_0 represents the value obtained by the simple kinetic argument. The extended Skyrme interaction GS2, mostly used in this paper (see Table I) leads to an effective mass $m^* = 0.65m$. Taken at face value, this effect alone will approximately double the mean-free path. (It may be argued that this value of m^* is too low, particularly in light of the energy brought into the system by a 100-MeV proton. An effective mass of $0.8m$ would correspond to an increase by a factor of 1.56. To allow for this uncertainty, we will use a factor of 1.8 in the present estimate.)

B. Density dependence

The explicit density dependence of the two-body interaction has a significant effect. For a Skyrme interaction with the parameters t_0, t_1, t_3, and t_4 (see Table I) satisfying the relationship $6t_4/t_3 \approx t_1/t_0$, the density-dependent part of the interaction has (approximately) the same range as the density-independent part. This results in a significant reduction of the scattering amplitude. We calculated the numerical value of the reduction for an interaction similar to (but somewhat simpler than) GS2. The quantity that governs this reduction is the ratio $t_3\rho/(6t_0)$. Since this ratio has the value ≈ -0.27 for GS2, the scattering amplitude will approximately be reduced by a factor $(1-0.27)=0.73$. The mean-free path is thus increased by a factor $\approx 1/(0.73)^2 = 1.9$. By contrast, if $t_4 = 0$, then the density dependence has no reductive effect on the mean-free path, since a zero-range repulsion has vanishing scattering amplitude.

C. Pauli principle

The important effect of the Pauli principle on the mean-free path has been stressed repeatedly by a large number of authors. One of the first thorough investigations of this effect was carried out by Clementel and Villi.[9] Neglecting the energy and angular dependence of the nucleon-nucleon cross sections, they obtained an explicit expression for the increase in the mean-free path due to the Pauli principle. Their result is written as

$$\lambda = \lambda_0 / F_0(R) . \tag{4}$$

The integral $F_0(R)$ is referred to as the "Pauli factor," and is given by simple calculation in the form

$$F_0(R) = \begin{cases} 1 - \frac{7}{5}R^{-1} + \frac{2}{5}R^{-1}(2-R)^{5/2} & \text{for } 1 \le R < 2 \\ 1 - \frac{7}{5}R^{-1} & \text{for } 2 \le R \end{cases} \tag{5}$$

with

$$R = k^2 / k_F^2 = (E+V)/T_F , \tag{6}$$

where k is the momentum of the incident nucleon, k_F and T_F are the Fermi momentum and kinetic energy, respectively, and V is the depth of the potential inside the nucleus. For $E = 100$ MeV, $V \approx 30$ MeV. Using $T_F = 35$ MeV, we obtain $R \approx 3.7$, and thus $F_0 \approx 0.62$. According to this simple estimate, the Pauli principle increases the mean-free path by about 50% at 100 MeV. Of course, the fractional increase gets larger with decreasing energy.

In this paper, the energy dependence of the cross section is explicitly taken into account as well. If the cross section as a function of the relative momentum can be written as

$$\sigma(k) = \sigma_0 + \sigma_1 k^2 + \sigma_2 k^4 \tag{7}$$

then the effect of the Pauli principle can be calculated separately for each of these terms and we get

$$\sigma_{\text{Pauli}}(k) = F_0 \sigma_0 + 4F_1 \sigma_1 k^2 + 16 F_2 \sigma_2 k^4 , \tag{8}$$

where F_0 is the "Pauli factor" (5). [The momentum integral in our general calculation, $I^{(1)}_{\tau_\alpha \tau_\mu}$ in (41) of Appendix B, is proportional to F_0 for symmetric nuclear matter. The detailed forms of the general quantities corresponding to F_1 and F_2 are also given in Appendix B.]

Combining these three effects, we estimate an increase of the mean-free path for a 100-MeV nucleon in symmetric nuclear matter by a factor of about $1.8 \times 1.9 \times 1.5 \approx 5$ over the "free-space" value. Our detailed calculations, presented in the subsequent sections of this paper, give an enhancement factor of ≈ 4 at 100 MeV. In light of the fact that the effects discussed above are not completely independent, the estimated value appears to be in reasonable agreement with the results of our calculations.

TABLE I. Several parameter sets of Skyrme interactions. Parameter set SII is from Ref. 20, Ska and Skb from Ref. 35, SGI and SGII from Ref. 36, GS1–GS6 from Ref. 16, and SkM from Ref. 37.

	t_0 (MeV fm³)	t_1 (MeV fm⁵)	t_2 (MeV fm⁵)	t_3	t_4 (MeV fm⁸)	x_0	x_1	x_2	x_3	x_4	W_0 (MeV fm⁵)	α_0
SII	-1169.9	585.6	-27.1	9331.1	0	0.34	0	0	1	0	105	1
Ska	-1602.78	570.88	-67.70	8000	0	-0.02	0	0	-0.286	0	125	$\frac{1}{3}$
Skb	-1602.78	570.88	-67.70	8000	0	-0.165	0	0	-0.286	0	125	$\frac{1}{3}$
SGI	-1603	515.9	84.5	8000	0	-0.02	-0.5	-1.731	0.1381	0	115	$\frac{1}{3}$
SGII	-2645	340	-41.9	15595	0	0.09	-0.0588	1.425	0.06044	0	105	$\frac{1}{6}$
GS1	-1268	887	-77.3	14485	-1853	0.15	0	0	1	1	105	1
GS2	-1177	670	-49.7	11054	-775	0.124	0	0	1	1	105	1
GS3	-1037	336	-7.3	5774	883	0.074	0	0	1	1	105	1
GS4	-1242	760	-146.2	19362	-2157	0.206	0	0	1	1	105	1
GS5	-1152	543	-118.6	15989	-1079	0.182	0	0	1	1	105	1
GS6	-1012	209	-76.3	10619	579	0.139	0	0	1	1	105	1
SkM	-2645	385	-120	15595	0	0.09	0	0	0	0	130	$\frac{1}{6}$

t_5(MeV·fm⁸)=0, x_5=0

III. THEORETICAL TOOLS

A. The Skyrme interaction and parameters

We will briefly discuss three versions of the Skyrme interaction,[21] usually referred to as conventional, generalized, and modified Skyrme interactions, respectively. The conventional Skyrme interaction[30] consists of terms corresponding to two-body and three-body interactions,

$$V = \sum_{i<j} v_{ij}^{(2)} + \sum_{i<j<k} v_{ijk}^{(3)} . \qquad (9)$$

The two-body and three-body interactions are taken as

$$v_{ij}^{(2)} = t_0(1+x_0 P_\sigma)\delta(\mathbf{r}) + \tfrac{1}{2}t_1[\delta(\mathbf{r})\mathbf{k}^2 + \mathbf{k}'^2\delta(\mathbf{r})]$$

$$+ t_2\mathbf{k}'\cdot\delta(\mathbf{r})\mathbf{k} + iW_0(\boldsymbol{\sigma}_1+\boldsymbol{\sigma}_2)\cdot\mathbf{k}'\times\delta(\mathbf{r})\mathbf{k} \qquad (10)$$

and

$$v_{ijk}^{(3)} = t_3\delta(\mathbf{r}_i - \mathbf{r}_j)\delta(\mathbf{r}_j - \mathbf{r}_k) , \qquad (11)$$

where $\mathbf{r} \equiv \mathbf{r}_i - \mathbf{r}_j$,

$$\mathbf{k} \equiv \frac{1}{2i}(\nabla_i - \nabla_j) \quad \text{acting to the right} , \qquad (12)$$

$$\mathbf{k}' \equiv -\frac{1}{2i}(\nabla_i - \nabla_j) \quad \text{acting to the left} . \qquad (13)$$

P_σ is the spin exchange operator and σ represents the Pauli spin matrices. The parameters of the conventional Skyrme interaction are denoted by t_0, t_1, t_2, t_3, x_0, and W_0.

The generalized and modified Skyrme interactions are *density-dependent* zero-range *two-body* interactions, which can be cast into a unified form known as the extended Skyrme interaction[19]

$$V = \sum_{i<j} v_{ij} , \qquad (14)$$

where

$$v_{ij} = t_0(1+x_0 P_\sigma)\delta(\mathbf{r}) + \tfrac{1}{6}t_3(1+x_3 P_\sigma)[\rho(\mathbf{R})]^{\alpha_0}\delta(\mathbf{r}) + \tfrac{1}{2}t_1(1+x_1 P_\sigma)[\delta(\mathbf{r})\mathbf{k}^2 + \mathbf{k}'^2\delta(\mathbf{r})]$$

$$+ \tfrac{1}{2}t_4(1+x_4 P_\sigma)[\delta(\mathbf{r})\rho(\mathbf{R})\mathbf{k}^2 + \mathbf{k}'^2\rho(\mathbf{R})\delta(\mathbf{r})] + t_2(1+x_2 P_\sigma)\mathbf{k}'\cdot\delta(\mathbf{r})\mathbf{k}$$

$$+ t_5(1+x_5 P_\sigma)\mathbf{k}'\cdot\delta(\mathbf{r})\rho(\mathbf{R})\mathbf{k} + iW_0(\boldsymbol{\sigma}_1+\boldsymbol{\sigma}_2)\cdot\mathbf{k}'\times\delta(\mathbf{r})\mathbf{k} \qquad (15)$$

with $\mathbf{R} \equiv (\mathbf{r}_i + \mathbf{r}_j)/2$. The quantities $t_i, x_i, i = 1, \ldots, 5$ and W_0 and α_0 are parameters of the extended Skyrme interaction. When $\alpha_0 = 1$, Eq. (14) specializes to the so-called generalized Skyrme interaction, while putting $t_4 = t_5 = 0$ reduces it to the modified Skyrme interaction. Several parameter sets of the extended Skyrme interaction are listed in Table I.

B. Green's function approach

This approach is based on the fact that the single-particle optical potential is equivalent to the self-energy of the single-particle Green's function,[31] in which the first-order self-energy contributes the main part of the real potential, while the second-order terms give the main contribution to the imaginary potential.[32] The corresponding first- and second-order diagrams are depicted in Fig. 1. A static potential is implicitly assumed (so that we deal with Goldstone diagrams[33]), and the diagrams drawn are meant to include both the direct and the exchange part of the interaction. The first-order diagram, Σ_{HF} represents the interaction with the mean field in the Hartree-Fock approximation. Here, we are mainly interested in the polarization diagram, Σ_{po} and the correlation contribution Σ_{co}. However, as we will see, it is necessary to calculate the mean field for both the single-particle energies (18) and the effective mass m^* (23). The analytical expressions for the diagrams in Fig. 1 read as follows:

$$V_{\text{HF}}(E) \equiv \Sigma_{\text{HF}}(k,E) = \sum_\mu n_\mu \langle \mathbf{k},\mathbf{k}_\mu | V | \mathbf{k},\mathbf{k}_\mu \rangle_A , \qquad (16)$$

$$\Sigma_{\text{po}}(k,E) = \tfrac{1}{2}\sum_{\mu\nu\lambda}(1-n_\mu)(1-n_\nu)n_\lambda |\langle \mathbf{k},\mathbf{k}_\lambda | V | \mathbf{k}_\mu\mathbf{k}_\nu \rangle|_A^2 /(E + e_\lambda - e_\mu - e_\nu + i\eta) ,$$

$$\qquad (17)$$

$$\Sigma_{\text{co}}(k,E) = \tfrac{1}{2}\sum_{\mu\nu\lambda}(1-n_\mu)n_\nu n_\lambda |\langle \mathbf{k},\mathbf{k}_\mu | V | \mathbf{k}_\nu\mathbf{k}_\lambda \rangle|_A^2 /(E + e_\mu - e_\lambda - e_\nu - i\eta) .$$

In Eqs. (16) and (17), the subscript A represents antisymmetrization and (at zero temperature considered here) $n_\mu = \theta(k_F - k_\mu)$, with the single-particle energies

$$e_\mu = \frac{\hbar^2 k_\mu^2}{2m_\mu} + V_{\text{HF}} , \qquad (18)$$

where V_{HF} stands for the Hartree-Fock mean field. Equations (16) and (17) can be evaluated in infinite nuclear matter using the extended Skyrme interaction (14). The details of this calculation are presented in Appendix A.
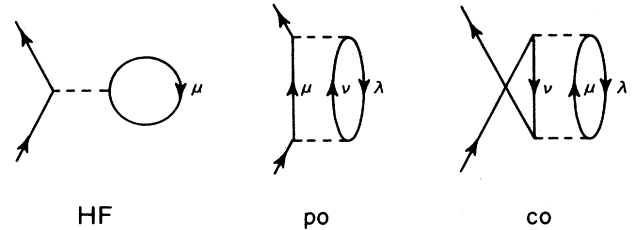

HF   po   co

FIG. 1. First- and second-order self-energy diagrams for the single-particle Green's function. HF presents the Hartree-Fock mean field, po and co stand for the polarization and correlation contributions, respectively. The diagrams include both the direct and the exchange parts of the interaction.

C. Imaginary potential and mean-free path

In the present approximation, the imaginary part of the optical potential is obtained by evaluating the second-order diagrams (17) in Fig. 1 with the extended Skyrme interaction (14). In order to carry out the integration, the principal integration formula

$$\frac{1}{(x+i\eta)} = \mathcal{P}\left[\frac{1}{x}\right] - i\pi\delta(x) \tag{19}$$

has been employed. Averaging over the spin and isospin variables enables us to write the imaginary potential in the form

$$W = \frac{1}{64\pi^5} \sum_{i=1}^{7} \{f_i[I_{\tau\tau}^{(i)}(k)+I_{\tau-\tau}^{(i)}(k)]+g_iI_{\tau\tau}^{(i)}(k)\} , \tag{20}$$

where f_i and g_i for $i=1,\ldots,7$ are combinations of Skyrme-interaction parameters and powers of the density ρ and $I_{\tau\tau'}^{(i)}$ for $i=1,\ldots,7$ denote the momentum integrals occurring. The detailed form of these quantities is given in Appendix B.

The mean-free path λ can be expressed in terms of the imaginary potential (20) with the help of the group velocity v_g:

$$\lambda = v_g\tau = \frac{\hbar v_g}{2W} , \tag{21}$$

where τ is the mean lifetime. The group velocity v_g describes the physical propagation of the wave packet representing a nucleon inside nuclear matter:

$$v_g \equiv \frac{dE}{\hbar dk} = \frac{\hbar k}{m^*} , \tag{22}$$

where the effective mass m^* is given by

$$m^* \equiv m\left[1 - \frac{dV_{HF}}{dE}\right] . \tag{23}$$

Equation (21) allows the calculation of the nucleon mean-free path in nuclear matter in terms of the effective mass m^* and the imaginary potential W (20). In order to connect to experimental information, we need a measure of the mean-free path in finite nuclei. In contrast to the experimental analysis of the data, where simple square wells have been used to represent the nuclei,[3] we wish to allow for more realistic density distributions. The price to pay is that a procedure is needed to get the mean-free path in finite nuclei from the nuclear matter values, and we resort to the local density approximation. The density distributons of finite nuclei are taken to have the usual Woods-Saxon shapes,

$$\rho(r) = \rho_0(1+\exp[(r-c)/a])^{-1} , \tag{24}$$

where, for definiteness, we fix the parameter values as[34]

$$\rho_0 = 3A[4\pi c^3(1+\pi^2a^2/c^2)]^{-1} ,$$

$$c = (0.978+0.0206A^{1/3})A^{1/3} \text{ fm} , \tag{25}$$

$$a = 0.54 \text{ fm} .$$

Assuming identical shapes for the proton and neutron distributions and taking $\rho_p/\rho_n = Z/(A-Z)$, the asymmetry parameter α characterizing nuclear matter [see Appendix A, Eq. (35)] can be identified as

$$\alpha = (A-2Z)/A . \tag{26}$$

Using the local density approximation in Eq. (21) yields a spherically symmetric distribution of the mean-free paths at a given incoming proton energy E. We will denote this distribution by $\lambda(E,r)$. Since experiments of course provide a "global" value of the mean-free path at a given energy in a given nucleus, we need to take a finite-nucleus average of $\lambda(E,r)$. It is physical to think about this average as first carried out along the beam direction and then transverse to the beam, but the same result can be obtained utilizing the spherical symmetry as

$$\bar{\lambda}(E) = \frac{3}{4\pi R^3} \int_0^R \lambda(E,r)4\pi r^2 dr \tag{27}$$

with

$$R = r_0 A^{1/3} , \tag{28}$$

where we have chosen $r_0 = 1.35$ fm (the value used in Ref. 3 to extract the mean-free path from the data) for the radius parameter. The sensitivity of the results to the upper limit of this integration will be discussed in the next section.

IV. RESULTS

The parameter set labeled GS2 in Table I has been used throughout the present calculation. In the following, we first illustrate the dependence of the results on the parameters characterizing the *infinite* nuclear medium the proton is moving in, and compare to another Skyrme interaction to convey the effect of different Skyrme parameter sets. We then turn to the mean-free path in finite nuclei and to comparisons to actual measurements. We focus on densities up to standard nuclear-matter density, and on the energy region between 50 MeV and ≈160 MeV, where good-quality data are available.

A. Mean-free path in nuclear matter

Figure 2 displays the dependence of the proton mean-free path on the density of nuclear matter at two different values of the asymmetry parameter α: the upper panel of the figure pertains to symmetric nuclear matter, while $\alpha = 0.2$ in the lower panel. The expected strong dependence of the mean-free path on the density is clearly seen. Above ≈100 MeV, the mean-free path increases with decreasing density. At low energies, however, the energy dependence of the nucleon-nucleon interaction becomes important, and (21) and (17) cannot be thought of as $\lambda \sim \rho^{-1}$. At sufficiently high densities the mean-free path decreases monotonically with increasing incident energy in the energy region considered, while a maximum appears at low densities.

The results for asymmetric nuclear matter are similar to the ones obtained for $\alpha = 0$. To bring out the difference, in Fig. 3 we display together the proton

PROTON MFP IN SYMMETRIC NUCLEAR MATTER

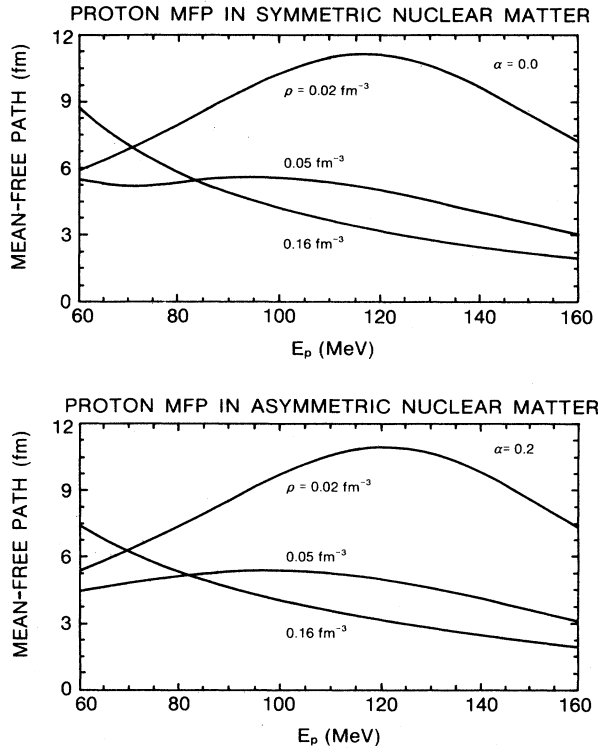PROTON MFP IN ASYMMETRIC NUCLEAR MATTER

FIG. 2. Calculated proton mean-free path in symmetric (upper panel) and asymmetric (lower panel) nuclear matter as a function of energy at three different densities. At around normal nuclear-matter density, the mean-free path decreases monotonically with energy, while it exhibits a maximum at low densities.

mean-free paths for $\alpha=0$ and 0.2 at nuclear matter density $\rho=0.16$ fm^{-3}. The two curves have the same shape, and converge at high energy. At energies below 100 MeV, the mean-free path in symmetric nuclear matter is
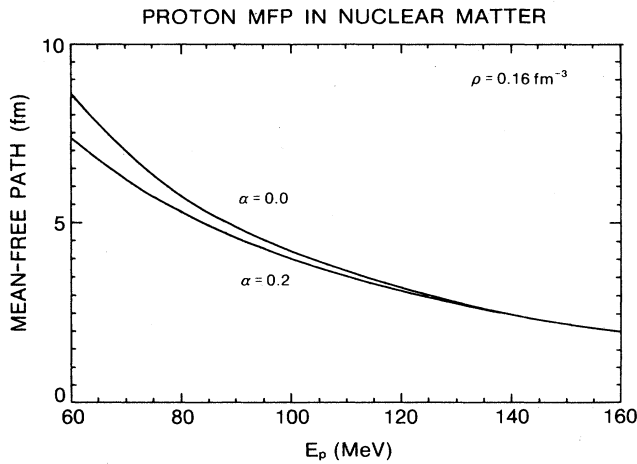
PROTON MFP IN NUCLEAR MATTER

FIG. 3. Calculated proton mean-free path as a function of energy at nuclear-matter density $\rho=0.16$ fm^{-3} for two different values of the asymmetry parameter α.
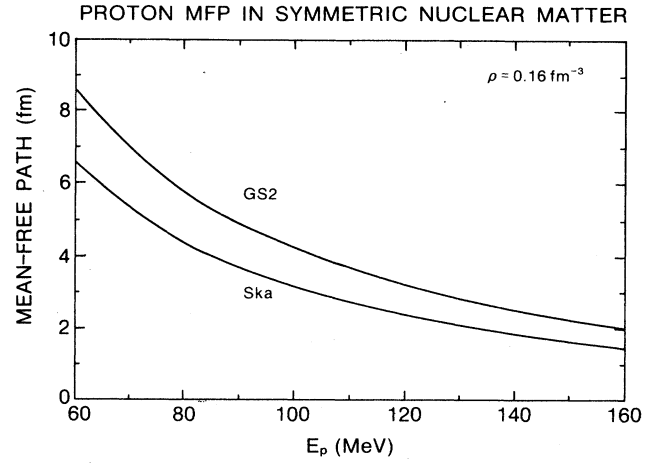
PROTON MFP IN SYMMETRIC NUCLEAR MATTER

FIG. 4. Calculated proton mean-free path in symmetric nuclear matter as a function of energy at nuclear-matter density $\rho=0.16$ fm^{-3} for two different Skyrme parameter sets given in Table I.

significantly longer than in the asymmetric case.

Figure 4 presents the results obtained with parameter set GS2 (the standard set for this work) and those obtained with the Skyrme interaction Ska (see Table I), for symmetric nuclear matter at density $\rho=0.16$ fm^{-3}. This figure serves to demonstrate that different Skyrme parameter sets result in differences of $\approx 1-2$ fm in the mean-free path in nuclear matter. In our calculations we use GS2, the parameter set which was preferred in Refs. 19 and 21 on the basis of good results for bound-state and optical-model calculations and which gives the longest mean-free path.

In general, the calculated results for the mean-free path in nuclear matter at normal density appear to be shorter than empirical values obtained from the analysis of scattering on finite nuclei. This is understandable, since nuclei have (more or less extended) surface regions, where the incoming proton has less matter to penetrate than in the bulk. This will be taken into account by performing a finite-nucleus average, as described in Sec. III.

B. Mean-free path in finite nuclei

As an example, we show in Fig. 5 the radial distribution of proton mean-free paths $\lambda(E,r)$ in ^{208}Pb as calculated in the local density approximation at several energies. As expected, the mean-free path takes on its bulk-matter value at $r=0$ (and in the interior), and diverges as r increases in the low-density surface region. Clearly, the finite-nucleus average (27) will be a sensitive function of the upper limit of the integral. The best one can do under these circumstances is to apply the radius parameter used in the analysis of the actual data we compare to. As mentioned above, we use the experimental radius parameter $r_0=1.35$ fm (Ref. 3) in Eq. (27). Admittedly, our results strongly depend on this choice, and so do the "experimentally determined" values of the mean-free path. A consistent rescaling, however, would not influence the
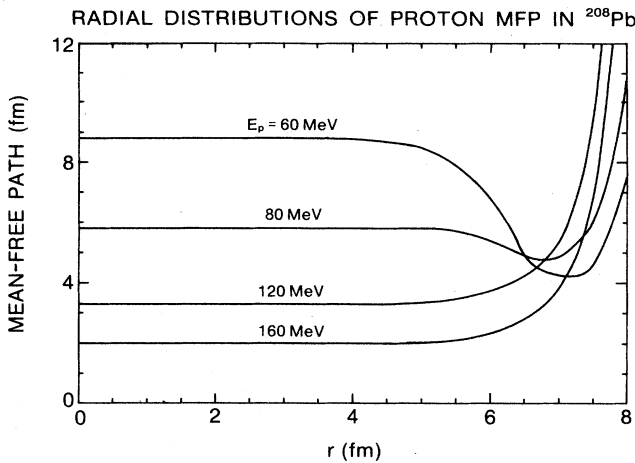
RADIAL DISTRIBUTIONS OF PROTON MFP IN ^{208}Pb

FIG. 5. Radial distribution of the proton mean-free path in ^{208}Pb in the local density approximation at different energies. The divergence as $r \to \infty$ is discussed in the text.

PROTON MEAN-FREE PATHS IN ^{90}Zr

FIG. 7. Average calculated proton mean-free path as a function of energy in ^{90}Zr (solid line). The experimental data represented by the symbols are determined from reaction cross sections (Refs. 1, 2, 4, and 5). The simple formula $\lambda_0 = (\bar{\sigma}\rho)^{-1}$ is also shown (dashed line).

quality of the agreement between the data and the calculations presented later in this paper.

Our final results for ^{40}Ca, ^{90}Zr, and ^{208}Pb are presented as the solid lines in Figs. 6, 7, and 8, respectively. We compare to data extracted mostly from reaction cross sections at different energies (symbols, from Refs. 1–5). The open circles represent values determined from optical-potential fits for ^{208}Pb.[3] Also shown are the results of the approximation $\lambda_0 = (\bar{\sigma}\rho)^{-1}$ (dashed lines) with $\rho = 0.16$ fm^{-3}. This simple formula (neglecting the Pauli principle and surface effects) severely underestimates the mean-free path in the entire energy range considered. On
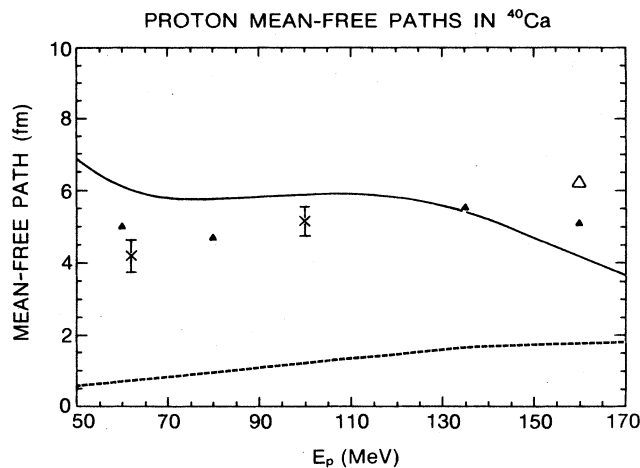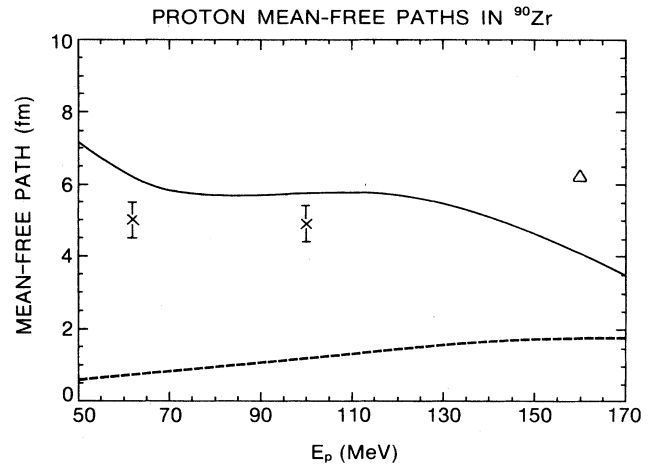
the other hand, the "data" scatter reasonably around the results of the calculation with the Skyrme interaction GS2, probably without a hint of the overall decreasing tendency of the mean-free path with energy displayed by our computation. Considering the uncertainties, however, it seems fair to extract a band of experimentally allowed mean-free paths from the data for each nucleus. Our results are consistent with such bands in the energy region considered.

We carried out the calculations with the additional Skyrme parameter sets listed in Table I. The mean-free paths obtained with the other parameter sets are too
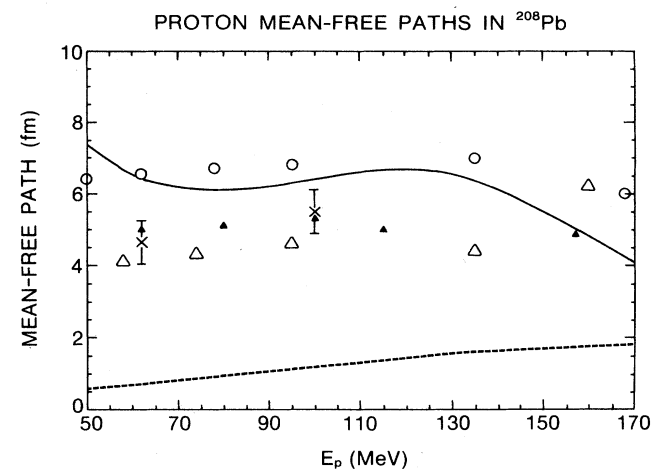
PROTON MEAN-FREE PATHS IN ^{40}Ca

FIG. 6. Average calculated proton mean-free path as a function of energy in ^{40}Ca (solid line). The experimental data represented by the symbols are determined from reaction cross sections (Refs. 1, 2, 4, and 5). The simple formula $\lambda_0 - (\bar{\sigma}\rho)^{-1}$ is also shown (dashed line).

PROTON MEAN-FREE PATHS IN ^{208}Pb

FIG. 8. Average calculated proton mean-free path as a function of energy in ^{208}Pb (solid line). The experimental data represented by the symbols are determined from reaction cross sections (Refs. 1, 2, 4, and 5) and from optical potential fits (Ref. 3). The simple formula $\lambda_0 = (\bar{\sigma}\rho)^{-1}$ is also shown (dashed line).

short (≈ 3 fm) in accordance with our earlier finding that GS2 yields the longest mean-free path in nuclear matter. Note also that in some of the other parameter sets t_4 has been set to zero for simplicity, in violation of the general relationship $t_3/t_0 \approx 6t_4/t_3$. The t_4 term gives a small contribution only, and including it is not expected to change the above general conclusion.

V. SUMMARY

In this paper, we demonstrated the usefulness of the extended Skyrme interaction (and, in general, of proper zero-range forces) in calculations of the mean-free path of a nucleon in the nuclear medium. The Green's function technique proved to be very efficient to incorporate the Pauli effect. Nonlocality enters in our calculations through the Pauli principle and through the effective mass. Together, these effects appear to resolve much of the discrepancy between the simple formula $\lambda_0 = (\bar{\sigma}\rho)^{-1}$ and experimental data, as pointed out earlier.[11,12] However, the large uncertainty in the data due to surface

effects should be kept in mind. Nevertheless, the present results are felt to provide further encouragement for the application of the extended Skyrme interaction in nuclear collision calculations.

APPENDIX A

In infinite nuclear matter, the nucleon wave functions can be taken as plane waves

$$\psi_{\mathbf{k}}(\mathbf{r}) = \frac{1}{\sqrt{\Omega}} e^{i\mathbf{k}\cdot\mathbf{r}} \chi_\sigma \chi_\tau , \tag{29}$$

where Ω is the normalization volume and χ_σ and χ_τ represent the spin and isospin parts of the wave function, respectively. Evaluating the mean field (16) with the wave functions (29) yields for the neutron and proton (distinguished by the index τ) potentials, respectively,

$$V_\tau = (m_\tau^*/m_\tau) \left| t_0[(1+\tfrac{1}{2}x_0)\rho - (x_0+\tfrac{1}{2})\rho_\tau] + \tfrac{1}{6}t_3\rho^{\alpha_0}[(1+\tfrac{1}{2}x_3)\rho - (x_3+\tfrac{1}{2})\rho_\tau] \right.$$
$$+ \frac{1}{40\pi^2}[t_1(1-x_1) + t_4\rho(1-x_4) + 3t_2(1+x_2) + 3t_5\rho(1+x_5)]k_\tau^5$$
$$\left. + \frac{1}{20\pi^2}[t_1(1+\tfrac{1}{2}x_1) + t_4\rho(1+\tfrac{1}{2}x_4) + t_2(1+\tfrac{1}{2}x_2) + t_5\rho(1+\tfrac{1}{2}x_5)](2k_F^3 - k_\tau^3)^{5/3} \right\} + (1 - m_\tau^*/m_\tau)E .$$

$$\tag{30}$$

Here E is the incident energy and the effective mass m^* is defined in Eq. (23). In terms of the Skyrme parameters,

$$\frac{m_\tau^*}{m_\tau} = \left[1 + \frac{m_\tau}{2\hbar^2}\{t_1[(1+\tfrac{1}{2}x_1)\rho - (x_1+\tfrac{1}{2})\rho_\tau] + t_4\rho[(1+\tfrac{1}{2}x_4)\rho - (x_4+\tfrac{1}{2})\rho_\tau] \right.$$
$$\left. + t_2[(1+\tfrac{1}{2}x_2)\rho + (x_2+\tfrac{1}{2})\rho_\tau] + t_5\rho[(1+\tfrac{1}{2}x_5)\rho + (x_5+\tfrac{1}{2})\rho_\tau]\} \right]^{-1} . \tag{31}$$

In Eqs. (30) and (31) the subscript τ stands for the isospin component. The densities and the Fermi momenta satisfy the standard relations

$$\rho = \rho_n + \rho_p \equiv \frac{2k_F^3}{3\pi^2} , \tag{32}$$

$$\rho_p \equiv \tfrac{1}{2}(1-\alpha)\rho \equiv \frac{k_p^3}{3\pi^2} , \tag{33}$$

$$\rho_n \equiv \tfrac{1}{2}(1+\alpha)\rho \equiv \frac{k_n^3}{3\pi^2} , \tag{34}$$

with the asymmetry parameter

$$\alpha \equiv (\rho_n - \rho_p)/\rho . \tag{35}$$

APPENDIX B

The imaginary potential W (20) is obtained from the second-order diagrams in Fig. 1. Averaging over the spin

and isospin indices allows the collection of the terms according to the momentum integrals $I_{\tau\tau'}^{(i)}$ with the coefficients

$$f_1 = 2[(1+x_0+x_0^2)t_0^2$$
$$+ \tfrac{1}{6}(2+x_0+x_3+2x_0x_3)t_0t_3\rho^{\alpha_0}$$
$$+ \tfrac{1}{36}(1+x_3+x_3^2)t_3^2\rho^{2\alpha_0}] ,$$

$$f_2 = \tfrac{1}{2}[(2+x_0+x_1+2x_0x_1)t_0t_1$$
$$+ (2+x_0+x_4+2x_0x_4)t_0t_4\rho$$
$$+ \tfrac{1}{6}(2+x_3+x_1+2x_3x_1)t_3t_1\rho^{\alpha_0}$$
$$+ \tfrac{1}{6}(2+x_3+x_4+2x_3x_4)t_3t_4\rho^{1+\alpha_0}] ,$$

$$f_3 = \tfrac{1}{8}[(1+x_1+x_1^2)t_1^2 + (2+x_1+x_4+2x_1x_4)t_1t_4\rho$$
$$+ (1+x_4+x_4^2)t_4^2\rho^2] ,$$

$$f_4 = \frac{1}{2}[(2+x_0+x_2+2x_0x_2)t_0t_2$$

$$+(2+x_0+x_5+2x_0x_5)t_0t_5\rho$$

$$+\frac{1}{6}(2+x_3+x_2+2x_3x_2)t_3t_2\rho^{\alpha_0}$$

$$+\frac{1}{6}(2+x_3+x_5+2x_3x_5)t_3t_5\rho^{1+\alpha_0}] , \quad (36)$$

$$f_5 = \frac{1}{8}[(2+x_1+x_2+2x_1x_2)t_1t_2$$

$$+(2+x_1+x_5+2x_1x_5)t_1t_5\rho$$

$$+(2+x_4+x_2+2x_4+x_2)t_4t_2\rho$$

$$+(2+x_4+x_5+2x_4x_5)t_4t_5\rho^2] ,$$

$$f_6 = \frac{1}{8}[(1+x_2+x_2^2)t_2^2$$

$$+(2+x_2+x_5+2x_2x_5)t_2t_5\rho$$

$$+(1+x_5+x_5^2)t_5^2\rho^2] ,$$

$$f_7 = \frac{1}{4}W_0^2 ;$$

$$g_1 = -\frac{1}{2}[2(1+4x_0+x_0^2)t_0^2$$

$$+\frac{2}{3}(1+2x_0+2x_3+x_0x_3)t_0t_3\rho^{\alpha_0}$$

$$+\frac{1}{18}(1+4x_3+x_3^2)t_3^2\rho^{2\alpha_0}] ,$$

$$g_2 = -\frac{1}{2}[(1+2x_0+2x_1+x_0x_1)t_0t_1$$

$$+(1+2x_0+2x_4+x_0x_4)t_0t_4\rho$$

$$+\frac{1}{6}(1+2x_3+2x_1+x_3x_1)t_3t_1\rho^{\alpha_0}$$

$$+\frac{1}{6}(1+2x_3+2x_4+x_3x_4)t_3t_4\rho^{1+\alpha_0}] ,$$

$$g_3 = -\frac{1}{16}[(1+4x_1+x_1^2)t_1^2$$

$$+2(1+2x_1+2x_4+x_1x_4)t_1t_4\rho$$

$$+(1+4x_4+x_4^2)t_4^2\rho^2] ,$$

$$g_4 = g_5 = 0 , \quad (37)$$

$$g_6 = \frac{1}{16}[(1+4x_2+x_2^2)t_2^2$$

$$+2(1+2x_2+2x_5+x_2x_5)t_2t_5\rho$$

$$+(1+4x_5+x_5^2)t_5^2\rho^2] ,$$

$$g_7 = \frac{1}{4}W_0^2 .$$

The momentum integrals entering the second-order diagrams can be written as

$$I_{\tau_\alpha\tau_\mu}^{(i)} \int d\mathbf{k}_\mu d\mathbf{k}_\lambda d\mathbf{k}_\nu h_i(\mathbf{k}_\alpha,\mathbf{k}_\mu,\mathbf{k}_\lambda,\mathbf{k}_\nu)$$

$$\times \delta(E+\epsilon_\mu-\epsilon_\lambda-\epsilon_\nu)$$

$$\times \delta(\mathbf{k}_\alpha+\mathbf{k}_\mu-\mathbf{k}_\lambda-\mathbf{k}_\nu) , \quad (38)$$

where

$$h_1 = 1 ,$$

$$h_2 = \frac{1}{2}(k_{\alpha\mu}^2 + k_{\lambda\nu}^2) ,$$

$$h_3 = \frac{1}{4}(k_{\alpha\mu}^2 + k_{\lambda\nu}^2)^2 ,$$

$$h_4 = \mathbf{k}_{\alpha\mu}\cdot\mathbf{k}_{\lambda\nu} , \quad (39)$$

$$h_5 = \frac{1}{2}(k_{\alpha\mu}^2 + k_{\lambda\nu}^2)(\mathbf{k}_{\alpha\mu}\cdot\mathbf{k}_{\lambda\nu}) ,$$

$$h_6 = (\mathbf{k}_{\alpha\mu}\cdot\mathbf{k}_{\lambda\nu})^2 ,$$

$$h_7 = (\mathbf{k}_{\alpha\mu}\times\mathbf{k}_{\lambda\nu})^2 ;$$

$$\mathbf{k}_{\alpha\mu} \equiv \mathbf{k}_\alpha - \mathbf{k}_\mu , \quad \mathbf{k}_{\lambda\nu} \equiv \mathbf{k}_\lambda - \mathbf{k}_\nu . \quad (40)$$

The domain of integration in Eq. (38) is confined by the relations $k_\mu \leq k_{\tau_\mu}$, $k_\lambda \geq k_{\tau_\alpha}$, $k_\nu \geq k_{\tau_\mu}$, $\tau_\lambda = \tau_\alpha, \tau_\nu = \tau_\mu$, where k_{τ_α}, k_{τ_μ}, k_{τ_λ}, k_{τ_ν} are the Fermi momenta.

First, momentum addition for particle pairs was carried out to simplify the integrals. This made it possible to integrate out certain variables while keeping careful account of the integration regions. After these manipulations, the integrals (38) can be carried out analytically to yield

$$I_{\tau_\alpha\tau_\mu}^{(1)} = \frac{2\pi^2}{15k_\alpha\beta_{\tau_\alpha}}[(5B_0+3k_{\tau_\mu}^2)k_{\tau_\mu}^3+2(-B_0)^{5/2}\theta(-B_0)] ,$$

$$I_{\tau_\alpha\tau_\mu}^{(2)} = \frac{\pi^2}{105k_\alpha\beta_{\tau_\alpha}^2\beta_{\tau_\mu}}\{[35B_0B_1+21(B_1+B_0B_2)k_{\tau_\mu}^2+15B_2k_{\tau_\mu}^4]k_{\tau_\mu}^3+2(7B_1-3B_0B_2)(-B_0)^{5/2}\theta(-B_0)\} ,$$

$$I_{\tau_\alpha\tau_\mu}^{(3)} = \frac{2\pi^2}{945k_\alpha\beta_{\tau_\alpha}^3\beta_{\tau_\mu}^2}\{[105B_0B_3+63(B_3+B_0B_4)k_{\tau_\mu}^2+45(B_4+B_0B_5)k_{\tau_\mu}^4+35B_5k_{\tau_\mu}^6]k_{\tau_\mu}^3$$

$$+2(21B_3-9B_0B_4+5B_0^2B_5)(-B_0)^{5/2}\theta(-B_0)\} ,$$

$$I_{\tau_\alpha\tau_\mu}^{(4)} = \frac{2\pi^2}{105k_\alpha\beta_{\tau_\alpha}}\{[35B_0B_6+21(B_6+B_0B_7)k_{\tau_\mu}^2+15B_7k_{\tau_\mu}^4]k_{\tau_\mu}^3+(7B_6-3B_0B_7)(-B_0)^{5/2}\theta(-B_0)\} , \quad (41)$$

$$I_{\tau_\alpha\tau_\mu}^{(5)} = \frac{\pi^2}{315k_\alpha\beta_{\tau_\alpha}}\{[105B_0B_8+63(B_8+B_0B_9)k_{\tau_\mu}^2+45(B_9+B_0B_{10})k_{\tau_\mu}^4+35B_{10}k_{\tau_\mu}^6]k_{\tau_\mu}^3$$

$$+2(21B_8-9B_0B_9+5B_0^2B_{10})(-B_0)^{5/2}\theta(-B_0)\} ,$$

$$I^{(6)}_{\tau_\alpha \tau_\mu} = \frac{2\pi^2}{945 k_\alpha \beta \tau_\alpha} \{ [105 B_0 B_{11} + 63(B_{11} + B_0 B_{12}) k_{\tau_\mu}^2 + 45(B_{12} + B_0 B_{13}) k_{\tau_\mu}^4 + 35 B_{13} k_{\tau_\mu}^6] k_{\tau_\mu}^3$$

$$+ 2(21 B_{11} - 9 B_0 B_{12} + 5 B_0^2 B_{13})(-B_0)^{5/2} \theta(-B_0) \} ,$$

$$I^{(7)}_{\tau_\alpha \tau_\mu} = \frac{2\pi^2}{945 k_\alpha \beta \tau_\alpha} \{ [105 B_0 B_{14} + 63(B_{14} + B_0 B_{15}) k_{\tau_\mu}^2 + 45(B_{15} + B_0 B_{16}) k_{\tau_\mu}^4 + 35 B_{16} k_{\tau_\mu}^6] k_{\tau_\mu}^3$$

$$+ 2(21 B_{14} - 9 B_0 B_{15} + 5 B_0^2 B_{16})(-B_0)^{5/2} \theta(-B_0) \} - I^{(6)}_{\tau_\alpha \tau_\mu} ,$$

where

$$\theta(x) \equiv \begin{cases} 1, & \text{if } x \geq 0 \\ 0, & \text{if } x < 0. \end{cases} \tag{42}$$

The combinations B_i in Eq. (41) are defined as follows:

$$B_0 = (\beta_{\tau_\alpha} k_\alpha^2 - \beta_{\tau_\alpha} k_{\tau_\alpha}^2 - \beta_{\tau_\mu} k_{\tau_\mu}^2)/\beta_{\tau_\mu} ,$$

$$B_1 = \beta_{\tau_\mu} H_1 + \beta_{\tau_\alpha} H_2 ,$$

$$B_2 = (\tfrac{7}{3}\beta_{\tau_\alpha} + \beta_{\tau_\mu})\beta_{\tau_\mu} ,$$

$$B_3 = B_1^2 - \beta_{\tau_\alpha}\beta_{\tau_\mu} H_1 H_2 ,$$

$$B_4 = [2(\beta_{\tau_\alpha}^2 H_2 + \beta_{\tau_\mu}^2 H_1) + \beta_{\tau_\alpha}\beta_{\tau_\mu}(H_1 + H_2)$$

$$+ 2\beta_{\tau_\alpha} B_1 + 4\beta_{\tau_\alpha}^2 \beta_{\tau_\mu} k_\alpha^2]\beta_{\tau_\mu} ,$$

$$B_5 = (\tfrac{23}{5}\beta_{\tau_\alpha}^2 + 3\beta_{\tau_\alpha}\beta_{\tau_\mu} + \beta_{\tau_\mu}^2)\beta_{\tau_\mu}^2 ,$$

$$B_6 = (k_{\tau_\alpha}^2 - k_{\tau_\mu}^2) - \tfrac{1}{2}B_0(\beta_{\tau_\alpha} - \beta_{\tau_\mu})/\beta_{\tau_\alpha} ,$$

$$B_7 = -\tfrac{1}{2}(\beta_{\tau_\alpha} - \beta_{\tau_\mu})/\beta_{\tau_\alpha} ,$$

$$B_8 = G_1 B_6 - G_3 B_0^2 ,$$

$$B_9 = G_2 B_6 + G_1 B_7 - 2 G_3 B_0 , \tag{43}$$

$$B_{10} = G_2 B_7 - G_3 ,$$

$$B_{11} = 3 B_6^2 + \tfrac{1}{4} S^2 B_0^2 ,$$

$$B_{12} = 4 G_1 - 4 k_\alpha^2 + 6 B_6 B_7 + \tfrac{1}{2} S^2 B_0 ,$$

$$B_{13} = 3 B_7^2 + 4S + \tfrac{1}{4} S^2 + \tfrac{4}{5} ,$$

$$B_{14} = 3(G_1 - k_\alpha^2) k_\alpha^2 ,$$

$$B_{15} = 5 G_1 + (3S - 2) k_\alpha^2 ,$$

$$B_{16} = 5S - \tfrac{7}{5} ,$$

with

$$H_1 = \beta_{\tau_\alpha} k_\alpha^2 + (\beta_{\tau_\alpha} - \beta_{\tau_\mu}) k_{\tau_\mu}^2 ,$$

$$H_2 = \beta_{\tau_\alpha} k_\alpha^2 - (\beta_{\tau_\alpha} - \beta_{\tau_\mu}) k_{\tau_\alpha}^2 \tag{44}$$

and

$$G_1 = \frac{1}{\beta_{\tau_\alpha} \beta_{\tau_\mu}} [(\beta_{\tau_\alpha} + \beta_{\tau_\mu})\beta_{\tau_\alpha} k_\alpha^2$$

$$- (\beta_{\tau_\alpha} - \beta_{\tau_\mu})(\beta_{\tau_\alpha} k_{\tau_\alpha}^2 - \beta_{\tau_\mu} k_{\tau_\mu}^2)] ,$$

$$G_2 = 4 + S , \tag{45}$$

$$G_3 = (\beta_{\tau_\alpha}^2 - \beta_{\tau_\mu}^2)/(6\beta_{\tau_\alpha}^2) .$$

Finally,

$$S = \frac{\beta_{\tau_\alpha} + \beta_{\tau_\mu}}{\beta_{\tau_\alpha}}, \quad \beta_{\tau_\alpha} = \frac{\hbar^2}{2 m^*_{\tau_\alpha}}, \quad \beta_{\tau_\mu} = \frac{\hbar^2}{2 m^*_{\tau_\mu}} . \tag{46}$$

For symmetric $(N = Z)$ nuclear matter these expressions simplify considerably. We find

$$\begin{aligned} B_0 &= k^2 - k_F^2 , \\ B_1 &= 2\beta^2 k^2 , \\ B_2 &= \tfrac{10}{3}\beta^2 , \\ B_3 &= 3\beta^4 k^4 , \\ B_4 &= 14\beta^4 k^2 , \\ B_5 &= \tfrac{43}{5}\beta^4 , \end{aligned} \tag{47}$$

and the first three $I_{\tau\tau}$ in (41) reduce to the following simple equations:

$$\begin{aligned} I^{(1)} &= c k F_0(R) , \\ I^{(2)} &= c k^3 F_1(R) , \\ I^{(3)} &= c k^5 F_2(R) , \end{aligned} \tag{48}$$

where $c = 2\pi^2 k_F^3/(3\beta)$, and the functions F_n are the quantities used in Eq. (8) with R defined as in Eq. (6). For $R = k^2/k_F^2 \geq 2$ we have

$$\begin{aligned} F_0(R) &= 1 - \tfrac{7}{5} R^{-1} , \\ F_1(R) &= 1 - \tfrac{2}{5} R^{-1} - \tfrac{9}{7} R^{-2} , \\ F_2(R) &= 1 + \tfrac{7}{5} R^{-1} - \tfrac{83}{35} R^{-2} - \tfrac{473}{315} R^{-3} . \end{aligned} \tag{49}$$

[1]J. P. Schiffer, Nucl. Phys. **A335**, 339 (1980).

[2]A. Bohr and B. R. Mottelson, *Nuclear Structure* (Benjamin, New York, 1969), Vol. 1.

[3]A. Nadasen, P. Schwandt, P. P. Singh, A. D. Bacher, P. T. Debevec, W. W. Jacobs, M. D. Kaitchuck, and J. T. Meek, Phys. Rev. C **23**, 1023 (1981).

[4]K. Kikuchi and M. Kawai, *Nuclear Matter and Nuclear Reactions* (North-Holland, Amsterdam, 1968).

[5]M. M. Giannini, G. Ricco, and A. Zucchiatti, Ann. Phys. (N.Y.) **208**, 124 (1980).

[6]H. Stöcker and W. Greiner, Phys. Rep. **137**, 278 (1986).

[7]C. Gregoire and B. Tamain, Ann. Phys. (Paris) **11**, 323 (1986).

[8]S. Nagamiya and M. Gyulassy, Adv. Nucl. Phys. **13**, 201 (1984).

[9]E. Clementel and C. Villi, Nuovo Cimento **2**, 176 (1955).

[10]J. P. Jeukenne, A. Lejeune, and C. Mahaux, Phys. Rep. **25**, 83 (1976).

[11]J. W. Negele and K. Yazaki, Phys. Rev. Lett. **47**, 71 (1981).

[12]S. Fantoni, B. L. Friman, and V. R. Pandharipande, Phys. Lett. **104B**, 89 (1981).

[13]C. Mahaux, P. F. Bortignon, R. A. Broglia and C. H. Dasso, Phys. Rep. **120**, 1 (1985).

[14]T. Cheon, Phys. Rev. C **38**, 1516 (1988).

[15]C. W. Wong (unpublished).

[16]S. Krewald, V. Klemt, J. Speth, and A. Faessler, Nucl. Phys. **A281**, 166 (1977).

[17]M. Waroquier, H. Heyde, P. van Isacker, and J. Vincx, Phys. Lett. **63B**, 9 (1979).

[18]M. Waroquier, H. Heyde, and G. Wenes, Nucl. Phys. **A404**, 269 (1983).

[19]W. Ye, H. J. Yuan, Q. Gao, Q. Shen, J. Zhang, R. Liu, and Y. Gu, Chin. J. Nucl. Phys. **7**, 166 (1985) [Chin. J. Phys. **6**, 139 (1986)].

[20]D. Vautherin and D. M. Brink, Phys. Rev. C **5**, 626 (1972).

[21]H. J. Yuan, W. Ye, Q. Gao, and Y. Zhou, Chin. J. Nucl. Phys. **8**, 216 (1987).

[22]J. Dabrowski, in *Condensed Matter Theories*, Proceedings of the 11th International Workshop on Condensed Matter Theories, Oulu, 1987, edited by J. S. Arponen, R. F. Bishop, and M. Manninen (Plenum, New York, 1988), Vol. 3, p. 311.

[23]B. A. Brown, W. A. Richter, R. E. Julies, and B. H. Wildenthal, Ann. Phys. (N.Y.) **182**, 191 (1988).

[24]R. Brugger and M. K. Weigel, Phys. Rev. C **35**, 2049 (1987).

[25]M. Lacombe et al., Phys. Rev. C **21**, 861 (1980).

[26]R. Machleidt, K. Holinde, and Ch. Elster, Phys. Rep. **149**, 1 (1987).

[27]A. Lejeune, P. Grange, M. Martzloff, and J. Cugnon, Nucl. Phys. **A453**, 189 (1986).

[28]J. W. Negele and D. Vautherin, Phys. Rev. C **5**, 1472 (1972).

[29]G. E. Brown and V. Koch, in Proceedings of the 8th High Energy Heavy Ion Study, Berkeley, 1987, edited by J. W. Harris and G. J. Wozniak (Lawrence Berkeley Report LBL-24580, 1988, p. 29).

[30]T. H. R. Skyrme, Nucl. Phys. **9**, 615 (1959).

[31]J. S. Bell and E. J. Squires, Phys. Rev. Lett. **3**, 96 (1959).

[32]Q. Shen, Comm. Theor. Phys. **2**, 1233 (1983).

[33]A. L. Fetter and J. D. Walecka, *Quantum Theory of Many-Particle Systems* (McGraw-Hill, New York, 1971).

[34]J. W. Negele, Phys. Rev. C **1**, 1260 (1970).

[35]H. S. Köhler, Nucl. Phys. **A258**, 301 (1976).

[36]V. G. Nguyen and H. Sagawa, Phys. Lett. **106B**, 379 (1981).

[37]H. Krivine, J. Treiner, and O. Bohigas, Nucl. Phys. **A336**, 155 (1980).